LASER WELDING - Literature Review

C.A. Walsh
Materials Science and Metallurgy Department, University of Cambridge, England. July 2002.

Note - This review is not comprehensive - the subject area is now vast. The sections on parameter modelling and temperature field calculations are the most complete parts of the review. A separate review on strength measurements and industrial standards has been carried and documented in a separate file.

1. Introduction

Lasers are now being used in the automotive industry to produce seam or stitch welds, as alternatives to conventional resistance spot welding, which are used extensively for attaching auto-body panels to sub-assemblies. The advantages of laser welding over resistance spot welding result from the smallness of the laser spot size, the large penetration depth of the weld into the material and the requirement that only single-sided access to the workpiece is necessary. Further, the equipment used to carry out the welds can be easily adapted to new vehicle program changes, unlike that used for resistance spot welding.[1] Potential benefits realised by the application of laser welding include reduced flange widths, increased structural strength and high speed automated processing. Traditionally CO_2 lasers have been used for auto body applications. Recent advances have been made with Nd:YAG lasers, which are now capable of producing beam powers of more than 2 kW or more through a fibre optic cable. This is particularly useful for robotic operations, where it is necessary to manipulate the laser beam about a stationary part. Lasers are also used in the manufacture of tailored blanks, where suitably prepared sheet metal, including differing thickness and material combinations, are butt welded together prior to being pressed into the finished shape. This results in considerable cost and weight savings and increases structural rigidity.[2]

Although at present steel is the main material used in the vehicle manufacturing industry, the use of lighter materials, such as Al, Mg and Ti will in the future become of increasing importance, in order to reduce weight. This, however, will require the ability to make satisfactory joins between these materials and steel.[3] Aluminium alloys are invariably less weldable than automotive sheet steels due to its high diffusivity and the presence of passive oxide layers, which have a significantly higher melting temperature than the base alloy and often a poorer electrical conductivity. Laser welding of Al alloys is also problematic due to its high thermal conductivity and high reflectivity of the laser light, but progress is being made using Nd:YAG lasers.[2]

A mixture of both laser welded and seam-mash welded blanks are currently being produced. Laser welds produce a cosmetically more appealing weld which is harder than the mash weld. Mash seams are easier to form, because of its lower hardness, but is thicker, which may limit its usefulness. Mash welds are wider than laser welds, which in some cases can inhibit formability. The cost of laser beam welding is now competitive compared with mash-seam welding. Both processes are capable of welding blanks at speeds of 4-10 m/min (67-167 mm/s). 1mm blanks can be welded at 7-10 m/min (117-167 mm/s); 2 mm and 1.5 mm blanks at 4.5-5 m/min (75-83 mm/s). The HAZ (heat affected area) for both laser and mash seam welds is relatively narrow (4-8mm). Due to their increased hardness, however, the seams need to be kept away from critical (high strain) areas. The harder the bead the more susceptible it is to fracture. Mild steel has hardness of about 110HV; mash seams in mild steel typically have hardness 160-180 HV. Planishing (flattening) of the mash seam increases its hardness to 200-240 HV. The hardness of laser welds, however, is somewhat greater - typically about 400 Vickers.[4]

1.1 Laser Welding Systems

There are a number of different laser welding systems available. CO_2 and Nd:YAG lasers are already in use in industry. Low power Nd:YAG lasers are used in the electronics industry. Rapid improvements in technology mean that diode lasers of sufficiently high power and power density for the production of good deep penetration welds are now available.

1.1.1 CO_2 lasers

These operate on a wavelength of 10.6μm and have a power range 1.5 - 6 kW, although some work at continuous power levels of 10kW and beyond. The energy absorption of the laser beam by metals is low, with an overall efficiency of up to 15%, although the energy transfer efficiency from the laser beam to the workpiece can be as much as 0.8.[5] The optical system consists of mirrors and ZnSe lenses. These lasers are used for sheet welding at high weld speeds.[6,7]

1.1.2 Nd:YAG solid-state laser

The operating wavelength is 1.06μm. Most have average powers of several hundred Watts with pulses of peak power 1-10 kW (although 1000 kW is possible). Lasers with continuous powers of up to 3kW are now commercially available. Metals also have a higher surface absorptivity at this lower wavelength. Their overall efficiency is about 3-5%. Unlike CO_2 lasers, the beam can be guided through flexible glass fibres, due to its smaller wavelength. This makes it attractive for 3-d operations combined with articulated arm type robots, providing greater flexibility, accessibility and lower costs. In comparison CO_2 lasers have to use a complicated mirror system. The optical lenses and fibre optics provide a source of well defined size and angular radiating cone, with an even (top-hat) energy distribution, in contrast to the gaussian energy distribution associated with a CO_2 laser source coupled to a mirror-based delivery system. Mechanical or electro-optical deflectors can be used to deflect or multiplex a beam to several locations; dielectric beam splitters allow the energy to be split for simultaneous action; all in combination with the use of optical fibres for relaying the (sub-)beam to the place of work. Simultaneous spot welding by Nd:YAG lasers has found wide use in the electronics industry; it is highly efficient and has the inherent advantage of minimising distortion and stress in the finished product.[6,7,8] It is also possible to shape the temporal power profile of each pulse at pulse repetition rates of up to several kHz.[9]

1.1.3 Excimer gas lasers

These operate in the UV region (*e.g.* 248nm and 193nm). They have efficiencies of 2-4% and produce short pulses (tens of nanoseconds duration) and very high peak powers (above 10^7 W). The production of a suitable optical system is difficult as there are few materials which are transparent to radiation at these wavelengths. The lifetime of the optical elements is low. They typically emit approximately rectangular beams of aspect ratio 2:3 and low beam quality (K<0.01) in both directions. It is not easy to focus the beam to a small spot. Such lasers have been used in lithography.[6] [Beam quality can be defined in terms of the K-factor. The minimum theoretical diameter r_o (of a focused gaussian laser beam) is given in terms of K, the focal length f and aperture D of the focusing optics and the wavelength of the laser light λ as

$$r_o = \frac{2\lambda f}{\pi K D}$$

K is 1 for a gaussian beam and less than 1 for other beam modes. Analogous systems uses the M^2 notation where $M^2 = 1/K$.]

1.1.4 Diode lasers

These lasers operate on a wavelength in the near infra-red region of the spectrum (*e.g.* 808nm), which is an advantage of these lasers when compared with the CO_2 or Nd:YAG lasers, as many metallic materials used in industry, such as Al, have a higher absorption coefficient in this region.[10] They have efficiencies of up to 50%. To produce high power beams it is necessary to shape and combine radiation from a large number of emitting diodes. This has necessitated the development of suitable optical systems, incorporating micro-optical elements and diffractive optical elements.[6] Currently available diode lasers have powers in the kW range (up to 2.5kW), but have a lower beam quality when compared with the CO_2 and

Nd:YAG lasers. Further improvements in power and beam quality are needed to improve their capability for deep penetration welding. The apparatus for high power diode lasers, however, is very compact. A multi-kW laser head is only the size of a shoe-box.[3] This lower weight and compact size of diode lasers gives them a major advantage over with the traditional CO_2 and Nd:YAG lasers; it enables them to be mounted directly onto robots and moved around easily. They also have lower cooling requirements and a higher lifetime (each diode: 5000-10000 hours). The size of this system is primarily limited by the size of the required cooling system and will not be significantly affected by further improvements in the semiconductor technology.[10] A table comparing CO_2, Nd:YAG and diode laser characteristics is given in reference 11.

1.2 The Laser Welding Process

When welding with a laser beam, it is necessary to differentiate between two forms of welding: heat conduction welding and deep penetration welding. Conduction welding occurs at lower power densities or higher welding speeds. The absorbed energy is transferred by heat conduction into the volume of the workpiece and produces a broad, shallow pool of molten material. In deep penetration welding, the laser beam is focused to a small spot and the power density can exceed $5x10^6$ Watts/m^2. Sufficient energy is input to vaporise the material and a vapour-filled channel is formed through which the laser energy penetrates deep into the workpiece. Deep seams are produced which increase the absorption efficiency and make greater use of the laser beam. The energy required to melt and vaporise the material depends on the physical properties of the material (absorption coefficient, heat conduction), the wavelength of the laser light and the properties of the surface of the workpiece. These welds typically have deep, narrow weld profiles, a small HAZ and little distortion.[12] As a result of the better energy utilisation and larger depth to width ratios of welds attainable with deep penetration welding, this is the prime method of welding used in industry with the conventional laser sources.

The laser beam has also been used to carry out other heat processes with materials: surface hardening; alloying and vapour deposition, which do not involve melting of the material and require lower power densities; drilling and cutting, at even higher power densities where material ablation occurs, resulting in the formation of holes and slits in a material. Typical power densities used for each of these processes are[13]:

Surface hardening	-	10^3-10^4 Wcm^{-2}
Chemical vapour deposition	-	10^3-10^4 Wcm^{-2}
Surface alloying and cladding	-	10^5-10^6 Wcm^{-2}
Surface melting and welding	-	10^5-10^7 Wcm^{-2}
Drilling and ablation	-	$>10^7$ Wcm^{-2}

1.3 Physics of Laser Welding

1.3.1 Conduction mode welding

Heat is absorbed from the laser beam through the top surface of the metal. Steady state conditions are reached quickly (~2.5ms). The heat input is balanced by losses through the metal by conduction. The aspect ratio of the weld is determined by thermal conduction and surface-tension-driven fluid flow in the weld pool. As the surface tension decreases with temperature, outward flow of the molten metal occurs.[14] Penetration depths are determined by heat conduction and convection in the weld pool.

1.3.2 Deep penetration mode welding

A high energy-density laser beam vaporises the workpiece during the welding process to form a hole (keyhole), which allows the laser beam to penetrate into the metal to produce a deep, narrow melt pool. The absorption of the laser beam increases drastically once the keyhole has formed, as multiple reflections of the laser light occurs within the hole until most has been absorbed by the metal. Only a fraction (typically 0.5-0.8) of the absorbed energy causes melting of the metal to occur, the rest is dissipated by thermal conduction into the base of the metal, radiation, or convection in the melt pool.[15] [Marangoni convection, or surface-

tension-driven convection, occurs in the melt pool. Fluid flows outwards from the centre of the weld pool along the upper surface to the outside edge and returns below the surface. Increasing beam power makes the fluid flow shallower but faster. Decreasing the beam diameter makes the flow deeper and faster.[16]] The amount of heat lost in these ways is a determining factor in the ultimate penetration depth of the weld. At low travel speeds the conduction loss through the base metal is very large.[15]

The pressure of the vapour in the keyhole contributes to the penetration by stabilising the keyhole and keeping it open for further penetration, while the surface tension tends to close it at the surface. At low travel speeds, however, the vapour cavity tends to collapse resulting in reduced penetration. A plasma forms above the surface of the workpiece due to the interaction of the laser beam with the metal vapour and also with atoms in the shielding gas. This absorbs laser beam energy, thus lowering the maximum attainable weld penetration. The plasma also acts like a lens and degrades the optical quality of the laser beam.[17]

A keyhole cavity is formed only if the beam is sufficiently intense. It is filled by gas or vapour, created by continuous evaporation of the material by the beam. The absorption of energy depends on the degree of ionisation and density and hence on the temperature. At low temperatures the absorption coefficient is proportional to the degree of ionisation and increases rapidly with temperature. At higher temperatures ionisation is essentially complete and the absorption coefficient decreases with increasing temperature, as a result of the lower electron and ion densities. This absorption is by inverse Bremsstrahlung. So at low beam intensities beam penetration is limited, whereas at high beam intensities the penetration grows with beam power.[18]

1.4 A Good Weld

A good weld is crack-free and has high strength and reliability.[19] Pore formation and alloying element loss are important concerns in laser welding of automotive aluminium alloys and must be minimised.[20] The size and shape of the weld pool and the hardness of the microstructure are both important factors. A fine-grain microstructure in the weld pool with a low increase in hardness is desirable. The quality of a laser weld is also related to the depth of penetration of the laser beam.[21] Reference 22 details laser beam weld specification for automotive sheet steel.

1.5 Weld Processing Parameters

There are a number of process parameters which affect the quality, size and properties of laser weld.[9] Experiments have been carried out using both continuous wave lasers and pulsed lasers. In the case of cw lasers, the only parameters relating to the laser beam are laser power, beam size and shape on the workpiece, position of the focal plane of the beam with respect to the surface of the workpiece, power density (power/beam size), wavelength of the laser beam, beam divergence (focal length of the focusing lens), and intensity distribution of the beam. For pulsed lasers there are in addition the parameters: pulse energy, pulse repetition rate, pulse duration, mean laser power (pulse energy x pulse repetition rate), average peak power (pulse energy/pulse duration), average peak power density (average peak power/spot area), pulse shape. Other important parameters are: the welding speed (seam and stitch welds), welding time (spot welds) and length of weld (stitch welds). The amount of power in the incident laser beam which is actually absorbed (rather than reflected) by the material is dependent on the material and surface properties. The amount then used to produce a melted weld pool depends on the heat capacity and flow characteristics. Material related properties include: heat capacity, heat conductivity, surface reflectivity, melting temperature, thickness of material, physical orientation of weld (vertical or horizontal). Another set of parameters are related to the gas used to shield the welding process: type of gas, flow rate of gas, angle of gas flow to workpiece, nozzle designs. This review will be confined to continuous wave lasers only.

2. Material and Surface Properties

2.1 Optical Properties

The optical properties of the material, the wavelength of the laser light and the surface roughness of the workpiece are the main factors which determine the energy fraction of the beam which is absorbed and penetrates to a thickness generally defined as the optical penetration depth. A high optical absorption coefficient at the operating wavelength of the laser greatly enhances this process. The operating wavelength, however, is a fixed quantity determined by the choice of laser source: CO_2 lasers have a wavelength of 10.6 μm; Nd:YAG lasers have a wavelength 1.06μm; diode lasers operate at 808nm. In the case of CO_2 and Nd:YAG lasers, the absorptivity of many materials is low at wavelengths of 10.6 μm and 1.06 μm, resulting in very low energy efficiencies for these welding systems (typically 5-10% for CO_2 lasers and 1-3% for Nd:YAG lasers[11]). The wavelength of diode lasers, however, lies close to the maximum value of the absorption coefficient of many metals.[12] This significantly increases the energy efficiency of the diode laser welding process to as much as 60%.[11] In the case of Al, in particular, 808nm coincides with a local absorption maximum.

The absorption of the laser beam by the workpiece is also affected by the surface condition of the material. Optically rough surfaces cause less specular reflection of the beam and more readily absorb the light energy. In deep penetration welding, the formation of a 'keyhole' also enhances the coupling between the incident laser light and the material, as multiple reflections of the scattered light occur within the confined space of the keyhole.[23] This process greatly increases the amount of light absorbed. For example, for A5083 Al alloy about 80% of the total incident power from a CO_2 laser beam was initially reflected back. Once the surface has melted and a keyhole formed, this dropped to about 4-8%.[24]

What factors affect the length of time taken for a keyhole to form and the delay before the absorption increase occurs? The higher the thermal conductivity the longer it takes for the surface to melt and the longer the reflected intensity stays high.[24] The type of shielding gases used (Ar, He and N_2) has little effect, as plasma initiation takes longer to occur.[24]

2.2 Thermal Properties

For materials with higher thermal conductivity the depth of the melt is larger and cooling rate faster.[25]

2.3 Energy Transfer Efficiency and Melting Efficiency

The absorption of the laser beam by the weldment is strongly dependent on the laser power and the position of the focused laser beam. Two parameters have been used as a measure of the efficient use of the laser power in the production of a weld: the energy transfer efficiency and the melting efficiency. These are defined in the following way for a welding speed V:[5]

Energy transfer efficiency = nett heat input / laser output energy: $\eta = \frac{q_i}{q_o}$.

Melting efficiency = energy for melting / nett heat input

$$= \frac{V}{q_i} \cdot \left[\Delta h_f + \int_{T_r}^{T_l} C_p(T) dT \right]$$

(The energy for melting consists of two components: heat of fusion and heat due to the temperature rise.) The energy transfer efficiency is known to depend on the laser beam power density (power and focus). The melting efficiency is affected by laser output power and travel speed. Measurements of these parameters have been made by Fuerschbach[5] for bead-on-plate welds (partial penetration) in relatively thick plates of

304 stainless steel, 1018 low-carbon steel and pure tin using a continuous power CO_2 laser beam and Ar shielding gas. The laser beam was focused onto the top surface of the metal. The spot size was varied by using different focal length lenses. This inevitably introduced another parameter - the divergence of the incident laser beam.

For all three materials, the energy transfer efficiency was found to increase non-linearly from about 0.2 to about 0.8 with power densities of 0.5 to 9 $MWcm^{-2}$, reaching a plateau above about 3 MW/cm^2. The energy transfer efficiency also increased slightly with decreasing spot size and increasing focal length of the focusing lens. This was probably due to a decrease in beam divergence, resulting in greater absorption through constructive interference in a thin liquid metal film on the walls of the keyhole. These variations could be taken into account by plotting the energy transfer efficiency as a function of *laser power density* × *focal length* (referred to here as *normalised power density*). A more universal method of normalisation would have been to divide by the relative aperture of the lens (lens diameter / focal length). However, in this case the lens diameter had a constant value of about 19.4mm.

Melting efficiency increased asymptotically with laser power. It increased with travel speed at low speeds and decreased at high speeds, indicative of an optimum travel speed for achieving maximum melting efficiency (0.48 for 2-d heat flow). The melting efficiency was also dependent on the properties of the base material. Two dimensionless parameters were introduced to normalise these results and take into account the different thermophysical properties of the base material. Rykalin's dimensionless parameter[26]:

$$R_y = \frac{q_i v}{\alpha^2 \delta h}$$

where q_i is the nett power into the workpiece, v is the travel speed, α is the thermal diffusivity at the *liquidus* temperature and δh is the enthalpy of melting. Christensen's dimensionless parameter[27]:

$$Ch = \frac{Av^2}{\alpha^2}$$

where A is the weld cross-sectional area. It should be noted that the volume of the fusion zone, V, should be dependent on the power and travel speed only ($V = Av\Delta t$), as $q_i = q_{cond} + \delta h \frac{dV}{dt}$, where q_{cond} is the power conducted away, and is consequently an important state variable in the design of control systems for fusion welding. The conductance term depends on the thermal gradients surrounding the weld pool and incorporates the melting efficiency. The volume (cross-sectional area) of the weld pool is easily measured and is a robust indicator of melting efficiency and the nett heat input. For constant speed welding, the cross-sectional area is directly proportional to the weld pool volume. The melting efficiency is then given by

$$\eta_m = \frac{Ch}{R_y} = \frac{vA\delta h}{q_i}.$$

A plot of Ch against R_y for all the data produced an excellent correlation with

$$\eta_m = 0.48 - 0.29\exp\left(\frac{-R_y}{6.8}\right) - 0.17\exp\left(\frac{-R_y}{59}\right)$$

This equation could be used to estimate accurately the size of weld for a given material, travel speed and nett power. It could also be used to obtain values for the energy transfer efficiency by measuring the cross-sectional area, provided travel speed and material properties are known. Once the energy transfer efficiency has been determined, the equation could be used to make accurate predictions of weld size for any combination of output power or travel speed, provided the laser intensity remains constant.

Their experimental results showed that there is a strong dependence of the energy absorption on both laser power and beam size on the workpiece. It is necessary, therefore, to ensure that neither laser power nor spot size vary appreciably. This could best be achieved by using a processing regime where the energy transfer efficiency is relatively insensitive to fluctuations in power and focus spot size.[5]

3. Factors affecting Weld Shape

3.1 Power Density

One of the most important parameters is the power density of the incident laser beam. This is defined as the *power of the laser beam* / *beam area on the upper surface of the workpiece*. The definition of the cross-sectional area of the laser beam is not always straightforward. Some lasers, such as the CO_2 lasers, have laser beams which are comprised of different TEM modes; the TEM_{00} mode, being the most prevalent, has a gaussian intensity distribution. The diameter of such a beam is defined as being where the intensity has dropped to $1/e^2$ of the intensity in the centre of the beam.[13] The Nd:YAG and diode lasers, however, if guided onto the workpiece through an optic fibre, produce a beam which has a top-hat intensity distribution and a well defined beam size.

3.2 Welding Speed

The welding speed obviously affects the energy input per unit volume of the workpiece. In order to produce a melt pool at all not only must sufficient energy to heat and melt the metal be supplied, but the rate of power input must exceed the power loss, primarily by conduction through the base metal. If the power input is excessive, however, complete penetration of the workpiece may occur, with loss of material through the lower surface (*melt through*), or even complete removal of metal under the beam (as in *cutting*). To achieve a good weld, therefore, it is necessary to balance the power input from the laser beam (power density) against the speed at which it is traversed across the workpiece. If the speed is too high for a given laser power, insufficient energy is absorbed to produce a large melt pool. If the speed is too low, large amounts of heat are wasted by conduction into the base metal. The melting efficiency (described in section 2.3) is indicative of the optimum use of energy for the production of a weld.[5]

The shape and quality of the weld is also affected by welding speed. As the speed increases, the welding mode changes from deep penetration welding to conduction welding. At high speeds conduction welding occurs and the weld pool is shallow. At low speeds (provided the power density is great enough) deep penetration welding occurs and the weld pool is very deep and narrow.[28] At too high a welding speed, the keyhole becomes unstable and non-uniform penetration occurs. Establishing a stable keyhole is important for the production of a good weld.

3.2 Laser Beam Divergence and Focal Plane

A further factor which affects the power density is the beam divergence. The laser beam is focused to a small spot by a lens. Changes in the position of this spot with respect to the surface plane of the workpiece clearly cause a change in the power density of the beam on the surface. The penetration depth and weld pool geometry is consequently greatly influenced by such variations. A defocused beam produces welds with a much lower penetration than one which is focused on the surface of the workpiece. When the defocus is such that the power density is close to the threshold for keyhole formation, a stable keyhole is not formed and the pool shapes can be very variable.[20] It has also been found that focusing in a plane *above* the surface results in a rapid reduction in penetration depth, but this is much less apparent with distance *below* the surface, within the material. A fairly constant penetration for defocus values of up to -2.5mm have been obtained using a 120mm focal length lens.[29] Tsukomoto *et al.*[30] found the penetration to decrease rapidly at defocus values greater than 2mm above the surface, and much more slowly for values <-2mm. The sharp reduction in penetration and weld pool size when the beam is focused above the surface was attributed to the high beam intensity in the region of the shielding gas and metal vapour. The gas absorbs energy from the beam and forms a plasma when the power density exceeds a critical value (see section 5 below); this process is less significant when the beam is focused below the surface of the material and the beam intensity above the surface is lower.[20]

Semak *et al.*[31] has performed calculations for simulating laser welding using a transient keyhole model. Of particular importance was the absorption coefficient of the gas plasma in the keyhole. The laser beam was assumed to have a Gaussian radial intensity distribution, and the plasma absorption coefficient assumed to depend only on the *z*-coordinate only and have a maximum located at some distance below the focal plane. Experiments were also carried out using a 1.65 kW Rofin Sinar 1200SM CO_2 laser to make bead-on-plate welds on 12.7 mm thick 304 stainless steel and 1018 carbon steel specimens. Helium gas was used as a shielding gas. It was found, both theoretically and experimentally, that deeper welds were produced when the focal plane lay *above* the surface (diverging beam) than when it lay below the surface (converging beam), provided the beam intensity at the surface was the same. This contradicts work by other researchers who have found that the penetration depth was greater when the focal plane lay below the surface. Depending on the processing conditions the maximum weld depth could be obtained with either a converging or diverging beam; the absorption in the plasma near the surface being the determining factor. The plasma absorption coefficient depends on beam *intensity* (it increases as beam intensity increases) and also on beam radius. This latter dependence is due to the restriction imposed by a narrow keyhole on the flow of gas and plasma out of it. Consequently, narrower beams produce in a narrower keyhole resulting in a higher free electron density in the keyhole and a higher plasma absorption coefficient. Calculations showed that if the plasma is assumed to be weakly absorbing, then maximum penetration is achieved when the focal plane lies below the sample surface. However, an increase in maximum plasma absorption coefficient resulted in a decrease in penetration depth and a shift in the position of the focal plane for maximum penetration towards the sample surface. Further increases in the absorption coefficient resulted in the optimum position of the focal plane lying above the sample surface. So at lower beam intensities the maximum penetration depth was reached when the focus was inside the sample and at high beam intensities maximum penetration was reached when the focal plane was at or above the surface.

The divergence of the laser beam results in the diameter of the spot increasing and the power density decreasing with distance above and below the focal plane of the spot. The beam intensity affects the strength of the coupling between the beam and the plasma above the workpiece, the fraction of laser power reaching the surface and the penetration depth of the weld. The focal length of the final focusing lens, which determines the beam divergence, and the position of the focal plane with respect to the surface of the workpiece are therefore important parameters in a laser welding system.

3.3 Experimental Measurements of Weld Shape

A detailed list of experimental measurements carried out using continuous wave lasers is given in table 1.

Ref.	Laser Type	Material	Weld Type	Shield Gas	Focal Length (mm)	Beam Size	Power Density (G/m^2)	Focal Plane (mm)	Welding Mode	Welding Speed (mm/s)	Weld Width	Penetration (mm)	Melt Area (mm^2)
20	2.6kW Nd:YAG	1 & 1.45mm thick plates of Al alloy 5182	bead on plate	He				-2 to -1 -1 to 0.5 0.5 to 1.5 1.5 to 2.0	unstable keyhole unstable conduction	63.5 63.5 63.5 63.5		0.4 to 1.0 0.9 to 1.0 1 to 0.4 0.4	
20	2.6kW Nd:YAG	1 & 1.45mm thick plates of Al alloy 5754	bead on plate	He				-2 to -1 -1 to 0.5 0.5 to 1.5 1.5 to 2.0	unstable keyhole unstable conduction	105.8 105.8 105.8 105.8		0.7 to 1.45 1.45 1.45 to 0.5 0.4	
19	1-1.5kW YAG	Fe and Al sheets	lap			0.8mm diameter						gets shallower	
29	2kW Nd:YAG	aluminised steel; 1 and 1.2mm thick	lap		100mm				keyhole	25 to 54		1.9 to 1.4	
12	1.4kW Diode	St14 steel; 0.8mm thick	I-seam? I-Naht		50	3.9 x 3.2 mm^2	0.113		conduction	16.7	2.9	complete penetration	2.3
12	1.4kW Diode	Al AA2195; 2mm thick	I-seam? I-Naht		50	3.9 x 3.2 mm^2	0.113		conduction	5.8	3	melt-through 1.8	~5
12	1.4kW Diode	Mg AM60B; 3mm thick	I-seam? I-Naht		50	3.9 x 3.2 mm^2	0.113		conduction	6.7	3	melt-through 3.4	
15	2kW CO_2	1018 carbon steel	bead on plate	He CO_2 Ar	127	gaussian beam?		top surface		0.4 to 20 0.4 to 20 0.4 to 20		4.5 to 0.4 3.5 to 0.2 1.8 to 0.1	
32	CO_2	AISI 1020 cold-rolled steel plates 6.35mm thick	bead on plate				4.3kW 4.0kW 4.0kW		keyhole	29.6 29.6 33.9	2.68 2.60 2.43	4.8 4.45 4.15	
32	CO_2	AISI 1020 cold-rolled steel plates 7.94mm thick	bead on plate				4.3kW 4.95kW 4.95kW		keyhole	68.6 68.6 80.0	2.73 2.83 3.00	4.67 5.17 6.17	
32	CO_2	AISI 1020 cold-rolled steel plates 9.53mm thick	bead on plate				5.3kW 5.3kW		keyhole	80.0 96.0	3.0 3.5	6.70 7.20	

Table 1

Effect of *increasing* power density or welding speed on the weld parameters for continuous wave lasers.

4. Weld Defects

A number of defects have been observed, but can often be controlled by a suitable choice of welding speed. Weld surface topography is affected by the presence of a number of weld defects: undercutting, slumping, humping, blow-holes, all of which adversely affect weld quality.

4.1 Types of Weld Defects

4.1.1 Pores in the weld pool

Pores in the weld pool are produced by the keyhole collapsing too quickly and not allowing the molten metal to flow into the centre of the keyhole before solidification takes place. They occur primarily in the root of the weld.[33] Instability of the keyhole formation has been shown to be the main cause of macro-porosity (holes >0.2mm in size) in some Al alloys.[20] When using pulsed lasers, the porosity tends to increase with increasing power density and pulse time.[14]

4.1.2 Cratering

When using pulsed lasers, the transition from conduction to keyhole welding is accompanied by more frequent occurrence of both occluded gas pores in the root and cratering of the top surface, particularly at higher power densities. In general, increasing the power density and pulse time results in a rapid increase in cratering.[14]

4.1.3 Undercutting

When the edge of the weld is lower than the centre of the weld, it is said to be undercut. The amount of undercutting is defined as the difference in height of the highest and lowest points on the top surface of the weld.[34] When using pulsed lasers irregular undercutting can occur as the weld speed is increased, resulting in a deformed weld bead or *ropey bead*. At even higher speeds the undercutting becomes consistent.

4.1.4 Humping

This is a longitudinal weld defect, characterised by a regular bumping and restriction of the weld face. The weld metal forms humps above the surface level of the workpiece (as shown below). It can occur at high speeds. The weld pool shape plays a significant role in the formation of humping. Full penetration is not a prerequisite for humping to occur.[8]

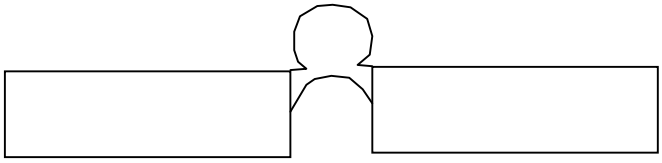

4.1.5 Blow-holes

Blow-holes sometimes form in the top weld bead, due to keyhole instabilities,[7] generally when the welding speed is too high.[35]

4.1.6 Drop

This is the depth to which the weld protrubes from the lower surface of the weld.[34]

4.1.7 Cracking

Cracks have been observed to formed mainly in the upper part of weldments.[33]

4.1.8 Non-uniformity and surface roughness

The surface roughness (on a micron scale) along the centreline of the top weld surface has been shown to be affected by welding speed, laser power, pulse duration and average peak power density of a pulsed laser.[35] Plots of roughness versus welding speed showed a minimum in the roughness at an optimum welding speed. As laser power was increased the sensitivity of the weld bead roughness to welding speed became less pronounced, and the size of roughness was generally lower. At too low a laser power the roughness

increased rapidly, which is indicative of thermodynamic instabilities in the weld pool. Increasing pulse duration increased weld roughness and reduced the range of acceptable welding speeds. For a given set of welding parameters, the travel speed for minimum roughness decreased as the mean laser output power was reduced, but increased with increasing pulse duration, due to the longer heating effect.[35]

4.1.9 Alloy loss and changes in chemical composition

Vaporisation of the material with preferential loss of the lower melting temperature elements can occur at high energy inputs. The welding speed has been found to have little effect on weld composition provided a stable keyhole had formed, showing that alloy loss is minimised once a stable keyhole is produced.[20]

4.1.10 Hardness

The weld pool has a considerably greater hardness than the original base metal. This can be due to a change in microstructure, formation of precipitates or the production of intermetallics (in the case of welds between dissimilar materials).[19]

4.2 Observed Weld Defects

Details of observed weld defects and the laser processing parameters are given in table 2.

Ref.	Laser Type	Material	Weld Type	Shield Gas	Beam Size	Power Density (G/m^2)	Focal Plane	Welding Mode	Welding Speed (mm/s)	Cratering	Porosity (Vol. %)	Cracking
20	2.6kW Nd:YAG	1 & 1.45mm thick plates of Al alloy 5182	bead on plate	He				melt through keyhole unstable	63.5 to 84.7 84.7 to 105.8 105.8 to 127		none 0 to 0.23 % 0.23 to 0.25 %	
20	2.6kW Nd:YAG	1 & 1.45mm thick plates of Al alloy 5754	bead on plate	He				keyhole unstable conduction	53 to 63.5 63.5 to 74 to 95 95 to 127		0 to .12 % 0.12 - 0.43 - 0 % none	
20	2.6kW Nd:YAG	1 & 1.45mm thick plates of Al alloy 5182	bead on plate	He			-2.0 to -0.5 -0.5 to 0.5 0.5 to 1.2 1.2 to 2.0	unstable keyhole unstable conduction	63.5		0 - 1.3 % 0 - 0.15 % 0.15 - 0.7 % none	
20	2.6kW Nd:YAG	1 & 1.45mm thick plates of Al alloy 5754	bead on plate	He			-2.0 to -1.0 -1.0 to 0.5 0.5 to 1.5 1.5 to 2.0	unstable keyhole unstable conduction	105.8		0 - 0.4 % 0.1 to 0.3 % 0.3 to 0 % none	
19	1-1.5kW YAG	Fe and Al sheets	lap joint		0.8mm							None at optimum speed.
29	2kW Nd:YAG	aluminised steel; 1 and 1.2mm thick	lap									
12	1.4kW Diode	0.8mm thick sheet of St14			3.9 x 3.2 mm^2	0.113		conduction	1m/min			

Table 2
Effect of *increasing* power density or welding speed on weld defects for continuous wave lasers.
keyhole = stable keyhole; unstable = unstable keyhole

5. Flow Rate and Type of Shielding Gas

Assist gases are needed to run most laser applications, either as a cutting gas, supporting the cutting process, or as a shielding gas, protecting a surface from the atmosphere during laser welding and surface treatment. It is also needed to control plasma formation during high-power laser welding and to protect the focusing optics from fumes and spatter.[36] He or Ar are generally used as shielding gases, as they are inert and do not react with the weld metal.

The high energy-density laser beam vaporises the workpiece during the welding process. Some of the vaporised metal atoms become ionised and forma a metal plasma just over the metal surface. Similarly, a plasma composed of shielding gas ions often forms above it, along the path of the laser beam. These plasmas absorb, diffuse and, if the critical electron density is reached, reflect the incident radiation, causing severe attenuation of the incident laser power (inverse Bremsstrahlung effect) and degrading the optical properties of the beam. This results in a lower quality weld and reduced penetration depth.[17,30] the plasma also emits radiation over a large spectral range, which contributes to surface heating, (particularly in the UV where the absorptivity of metal is high).[23] The increased scattering of the beam over the top surface is responsible for producing welds with cross-sectional shapes which resemble a nail-head, with a wide upper section and a narrow, parallel-sided lower section. Narrow, straight-sided melt pools have been produced by a CO_2 laser, operating under partial vaccum, which suppressed plasma formation.[37]

The absorption of the laser energy in the gas plasma has been confirmed experimentally to be caused by inverse Bremsstrahlung.[20] Assuming $\hbar\omega << kT_e$, the absorption coefficient α (m^{-3}) is obtained by

$$\alpha = 1.22\times10^{-39}\frac{Z^2 N_e N_i}{T_e^{3/2}}\ln(1.655\times10^{-3}T_e)$$

$$I_1 = I_o \exp(-\alpha x)$$

where Z is the ion charge, ω the angular frequency, T_e the electron temperature, N_e the elctron density, N_i the ion density, I_1 the transmitted power, I_o the incident laser power and x the plasma length.

In CO_2 laser welding a gas plasma has been observed to form only when the laser power exceeds a critical density of about $6.6\times10^5 W/cm^2$. The precise value depended on gas flow rate and increased with flow rate.[30] The effect of shielding gas on penetration depth has been investigated using a 2kW CO_2 laser to produce bead on plate welds in AISI 1018 carbon steel at various welding speeds (1-35 cm/s).[15] The observed penetration depths are given below as a percentage of the theoretical maximum possible depth:

Shielding Gas	**Observed Penetration Depth (% of theoretical maximum)**
He	20%
CO_2	10-18%
Ar	4-8%

The attenuation factor was constant for a given shielding gas for the range of welding speeds tested here, though this is not necessarily true for all laser conditions.

Plasma formation is usually avoided by the use of a gas stream directed at an angle onto the molten surface. However, determination of the appropriate nozzle diameter and angle of flow is often difficult. The penetration depth of the welds has been found to decrease with decreasing flow rate (from 70 to 10 l/min), particularly in the case of Ar as the shielding gas.[30] This is caused by an increase in the size of the gas plasma plume.

One effective gas flow system that has been proposed had many small orifices which produced a turbulent flow of gas both above and below the workpiece. The only parameter which needed to be adjusted and controlled was the gas flow rate. It's disadvantage was its high gas consumption. For an Ar flow rate>20 litres/min the plasma was inhibited completely. Welds with no pores or other defects could be produced with

a CO_2 laser. When using He as the shielding gas, sound welds could be made at high speeds (2.5-4.75 m/min) in plates of thickness 1.25, 0.75 and 0.5mm.[17]

As the plasma formation is a function of laser power density,[30] it is important to ensure that the laser beam is not brought to a focus *above* the plane of the specimen. The weld pool size has been observed to be greater when the beam is focused within the plate; the lower beam intensity above the plate results in less absorption by the formation of a plasma in the gas phase above the plate.[20]

The choice of shielding gas depends on *e.g.* gas shielding device, laser power and intensity, material thickness and quality requirements. He is better at suppressing plasma formation and is generally used for CO_2 laser welding. Ar is generally used for Nd:YAG laser welding.[36]

6. Heat Flow in Laser Welding

There are many theoretical models for calculating the heat flow and temperature distribution in welds, all involving simplifying assumptions of some sort. The governing differential equation of heat conduction is:

$$\frac{\partial T}{\partial t} = \frac{\partial}{\partial x}\left(\frac{\lambda}{\rho c}\cdot\frac{\partial T}{\partial x}\right) + \frac{\partial}{\partial y}\left(\frac{\lambda}{\rho c}\cdot\frac{\partial T}{\partial y}\right) + \frac{\partial}{\partial z}\left(\frac{\lambda}{\rho c}\cdot\frac{\partial T}{\partial z}\right) + q$$

where T is temperature, t is time, k is the thermal conductivity, c is the specific heat capacity, ρ is the density and q is the rate of heat supply per unit time.[38] This equation has been solved by Rosenthal for a moving point source on the surface of a semi-infinite medium, with the assumption that the material physical properties are not temperature dependent:

$$T(x,y,z) = T_o + \frac{q}{2\pi kR}\exp[-\frac{v}{2\kappa}(\xi + R)] \qquad \xi = x - vt \qquad R = \sqrt{\xi^2 + y^2 + z^2}$$

and a moving line source:

$$T(x,y) = T_o + \frac{q'}{2\pi k}\exp[-\frac{v\xi}{2\kappa}]K_0\left(\frac{vR}{2\kappa}\right) \qquad R = \sqrt{\xi^2 + y^2}$$

The solution for a moving line source assumes a constant line strength over depth: q'(W/m). κ is the thermal diffusivity ($k/\rho c$), v is the velocity of the point source and T_o is the ambient temperature. The latter solution gives a 2-d temperature field which is a reasonable approximation for a laser beam fully penetrating a thin metal sheet.

Rosenthal also considers the effect of finite thickness but shows that at distances larger than the thickness, the solution is similar to that for a 2-d line source in an infinite medium.

6.1 Analytical Solutions

Many welds are broader at the top than at the base of the weld (a 'nail-head' bead profile). Calculations by Ion[54] indicate that melt flow occurs at the top of the keyhole, as a result of a recoil pressure gradient, which carries heat from the centre part of the pool to the periphery, resulting in additional melting to get the familiar wine-glass shape. (However, our experiments show no wine-glass shape in the absence of shielding gas, so shielding gas and the gas plasma must be playing an important role in the formation of the nail-head shape.) Ion used a balance of line and point sources to represent the heating effects of the keyhole and the surface plasma respectively, and model the 'nail-head' bead profile.

Other people have approximated the laser source to a series of point sources. Lampa *et al.*[39] used a series of point sources with an enhanced value of the thermal conductivity in the upper part of the weld

region to account for the Maragoni flow in the weld pool, which increases lateral thermal transport and thereby causes a widening of the weld pool. The strength of the 'line' source was assumed to decrease linearly with depth and a larger value for the conductivity was used at the top. The strengths of the point sources were calculated to match the experimental weld profiles. The inclusion of the Maragoni effect is important for predicting the penetration depth. This thermocapillary flow has a diminishing influence on the heat distribution in the weld zone as the welding speed is increased, the effect becomes insignificant for speeds greater than 4 m/min (66 mm/s).

Steen *et al.*[40] used Rosenthal's line source solution with a point source on the top surface to model the broadening of the weld in the upper layer. The results were used to model experimental weld shapes. Akhter *et al.*[41] used the solution for a moving point source to derive a solution for a line source, where the source strength varies along the length of the line. This solution was used to model the shape of the fusion zone. Resch *et al.*[42] also used Rosenthal's solution for a point source and integrated over a line of point sources. Hilton[43] calculated the temperature distribution using an analytical solution to the heat conduction equation and determined the weld pool profile from the shape of the melting isotherm. The keyhole radius, as a function of depth down the weld, could also be calculated.

Tsai and Kou[44] used the line source solution but with a strength which obeyed Beer Lambert's law, so the power absorbed at a depth z is given by

$$-\frac{dI}{dz} = q(z) = \beta I_o e^{-\beta z}$$

where β is the absorption coefficient and I_o is the power of the beam at z=0. They provided an analytical solution for this case, however, which did produce a widening of the weld shape near the top, but the broadening was less than that observed experimentally. Beer Lambert's law describes a cross-section for energy absorption which remains constant throughout the depth of the material. Tsai and Kou then go on to introduce a modified version of Beer Lambert's law in which the cross-section does not remain constant with depth:

$$-\frac{dI}{dz} = q(z) = \beta(I_o - \int_0^g \gamma\, dz)\, e^{-\beta z} + \gamma$$

If γ=0 then Beer Lambert's law is recovered. When γ=I_0/g=constant, then it is equivalent to a uniform line source. They consider the case of a constant value for γ and produce an analytical solution. Increasing β or decreasing γ resulted in more power being absorbed near the top of the weld.

Metzbower *et al.*[45] used the results of Tsai and Kou to model the shape of the fusion zone. Calculations of the thermal profile at the centre of the weldment gave the cooling time from 800 to 500 deg.C as being about 1.6 seconds for a 12 kW CO_2 laser with a spot size of 3.56 mm and a travel speed of 11 mm/s and a He shielding gas. A conductivity of 31 W/m/K was used. The calculated cooling curves were essentially identical for distances of up to 1mm from the centre of the weld.

Lankalapalli *et al.*[32,46] used a 2-d analytical solution to the problem of heat flow from a cylindrical heat source to solve the problem of a 3-d conical shaped heat source (the keyhole). As the keyhole is conical, the amount of heat absorbed per unit depth decreased with depth. Heat losses from the top and bottom surfaces were ignored and heat conduction in the z-direction was neglected. The temperature distribution was obtained by integrating the 2-d solution over the depth of the keyhole. The strength of the heat source with depth was expressed in terms of the Péclet number (va/2α), where v is the speed, a the radius of the keyhole and α the thermal diffusivity. A semi-empirical expression for the keyhole size was given in terms of the Péclet number and weld width for low-carbon steels. The penetration of the weld was used as an initial estimate of the depth of the keyhole line source. The equation for the temperature distribution was evaluated to obtain the evaporation and melting isotherms which gave the keyhole and weld shapes. The temperature distribution was used to relate the temperature on the bottom surface with the penetration depth. Calculated depths were compared with experimental penetration depths for bead-on-plate welds on AISI 1020 cold-rolled steel (low C steel) of thicknesses 0.6-1cm.4-5.3kW Rofin Sinar 6000 laser; welding speeds 2-3.4cm/s. Good agreement was obtained for most welds, although in some cases the depths were overestimated by up

to 25%. The measured temperature was a function not only of penetration but also factors such as weld bead width, welding speed and measurement location. The source of errors included assumed keyhole shape, fluid flow in the molten pool, latent heat effects, sensor-sample distance and alignment.

6.2 Numerical Modelling

Numerical solutions to the heat conduction equation were able to consider more complex aspects of the problem such as radiative and convective heat losses from the surfaces and convection due to heat flow.[28]

Phanikumar *et al.*[28] modelled the welding procedure in a weld between dissimilar metals by considering the melting and mixing of the fluid forming the weld pool when a gaussian heat input was applied to the join between the workpieces. The coupled continuity, momentum, energy and mass-fraction equations along the boundary were solved numerically. Radiative and convective heat losses on the top and side surfaces were taken into account. Heat transfer occurred at the interface due to the different heat capacities and temperature gradients. Convection caused a heat flow to occur to move hot fluid to the cooler outer edges of the weld pool. The computations were carried out for a stationary spot welding and agreed qualitatively with experimental results from a weld between a piece of Ni and Cu.

Kar *et al.*[47] obtained numerical solutions of the equation governing heat conduction and fluid/gas movement at the solid/liquid and liquid/gas interfaces. They considered conservation of energy and mass and fluid convection in the model to obtain values for the free surface velocity, the keyhole depth and the weld width and depth. They concluded that the temperature gradient is higher in the trailing edge side of the keyhole. Dowden *et al.*[48] also considered fluid flow around the keyhole and also showed that at the rear of the keyhole a considerable drop in temperature can occur. For some metals, including iron, the temperature may not be far off the freezing temperature.

Resch *et al.*[42] used the solution for a moving point source at radius R (from Rosenthal):

$$T(x,y,z) = T_o + \frac{q}{2\pi kR}\exp[-\frac{v}{2\kappa}(\xi + R)] \qquad \xi = x - vt \qquad R = \sqrt{\xi^2 + y^2 + z^2}$$

where κ is the thermal diffusivity, v is the velocity of the point source and T_o is the ambient temperature. This equation was used to calculate the temperature field of an extended source by integrating over a series of point sources of specified strength along a path down to a depth equal to the penetration depth. As the penetration depth was not known, an algorithm was used to carry out the calculations iteratively to provide a self-consistent value for the final depth of the laser beam. The material properties were assumed to be constant. The calculations were carried out numerically using the algorithm and a mesh for welds in 2 mm thick mild steel at a speed of 3 m/min (50 mm/s) with an absorption coefficient of 0.3. A 500 W beam produced a penetration of 0.5mm with 3-d heat conduction. At 1.5kW the transition from conduction to keyhole welding occurred with a penetration of 1.7mm. 3-d conduction occurred at the bottom of the weld, but conduction was almost planar in the upper region. A deep keyhole was produced for a 2kW beam; the result being similar to that from the 2-d heat conduction equation for a moving line source. Plasma arc augmented welding was modelled by superimposing two heat sources: a line source for the keyhole formation by the laser beam and one of decreasing intensity with depth for the heat input from the plasma. This simulates the widening of the melt pool at the top. They also considered twin welding (a laser beam from either side of the workpiece) and showed isotherms for a laterally inclined weld (12 deg.).

6.3 Cooling Rate of the Weld Pool

Goldak *et al.*[49] used a finite element analysis for calculating the temperature field and cooling curves. A gaussian distribution of the heat source was assumed which had a double elliptical shape. A comparison of results with experiment and with Rosenthal's heat source calculations gave the following results for the cooling time from 800 to 500 °C:

Experiment:	1.9 s	19mm thick plate; 10mm penetration; e-beam weld; 2.8 kW; 5.3mm/s; 0.24% C steel.
Rosenthal 2-d solution:	2.4 s	con.=41W/m/K; cap.=4.5×10^6J/m^3/°C:; η=0.85
Rosenthal 3-d solution:	1.4 s	con.=41W/m/K; cap.=4.5×10^6J/m^3/°C:; η=0.85
Finite element analysis:	2.0 s	

Doong *et al.*[50] gave the following experimental measurements of the surface temperature of butt welds in AISI 1045 steel and AISI 304 stainless steel using a 2.5kW CO_2 cw laser with a gaussian TEM_{00} mode laser beam:

AISI 304 stainless steel: thickness 2mm; laser power 1.5kW.

Welding speed (mm/s):	6.67	10.0	16.67	23.33
Cooling rate (°C/s):	292	425	693	757
Time to cool 500-800 °C:	1.03	0.71	0.43	0.40

AISI 1045 steel: thickness 2.6mm; laser power 1.5kW.

Welding speed (mm/s):	6.67	10.0	13.33
Cooling rate (°C/s):	385	479	570
Time to cool 500-800 °C:	0.78	0.63	0.53

Zambon *et al.*[51] calculated the cooling curves for CO_2 laser welds in stainless steel using an analytical model. (Details of the calculations were given in another paper.) Calculations for a weld in a 2.1 mm thick sheet of UNS S 31803 steel with a 3 kW power laser (conductivity=25 W/m/K, diffusivity = 7×10^{-6} m^2/s, density=7858 kg/m^3, heat capacity=454.5 J/kg/K) gave a cooling rate of 1950 °C/s at 700 °C, whilst the time to cool from 800 to 500 °C was about 0.2 seconds. [My calculations using Rosenthal's line source model for the same parameters gives values of 2 seconds for a transfer efficiency of 0.57 and 6.2 seconds for a transfer efficiency of 1 second!]

Ion *et al.*[52] used Rosenthal's solution for a point source moving along a surface and extended it to consider a circular disc source moving along the surface. This did not affect the time taken to cool from 800 to 500 °C.

Grabás *et al.*[53] used a semi-analytical method for calculating a 3-d temperature field. They produce a solution for a plate of thickness L with a moving gaussian heat source distributed over a depth L'. (Details of the calculations were given elsewhere.) The material properties were assumed to be temperature independent. Some experimental cooling rates were given which showed a temperature increase in the 800 to 500 °C region. The time taken to cool from 800 to 500 °C agreed fairly well with their calculated values as shown in table 3.

Power (W)	Absorbed Power (W)	Speed (mm/s)	Speed (m/min)	Sheet Thickness (mm)	Δt (800-500 °C) Experiment	Theory
498	241	33	2	0.7	0.18	0.18
1766	1404	25	1.5	3	0.46	0.50
1440	1181	25	1.5	3	0.46	0.34

Table 3
Experimental and theoretical cooling times for several different laser processing times as given by Grabás *et al.*[53]

7. PARAMETER MODELLING EQUATIONS

7.1 Swift-Hook and Gick

Swift-Hook and Gick[54] solved the 2-d heat line source problem with heat input per unit depth = Q/g, where g is the penetration depth, and got the solution for the melting isotherm. They did, however, consider the temperature dependence of the conductivity k and express the solution in terms of the parameter

$$S = \int_{T_o}^{T_M} k dT$$

(For iron: 5.93x10^4 J/m/s, using a melting temperature T_M of 1371 °C.) From the solution a relationship between the parameters, speed, power, weld width and penetration depth can be expressed. The expressions are related in terms of the parameters X and Y:

$$Y = \frac{speed \times width}{mean\, diffusivity} = \frac{vw}{\overline{D}} = \frac{v(mm/s) \times w(mm)}{8.33} \qquad X = \frac{power}{penetration \times S} = \frac{Q}{gS} = \frac{Q(W)}{59.3g(mm)}$$

(Using mean values for the density (7651 kg/m^3), heat capacity (686 J/kg/K) and thermal conductivity (43.7 J/m/s/K), a mean value for the thermal diffusivity $\overline{D}$ is 8.33x10^{-6} m^2/s.) The asymptotic expressions for large Y and small Y are given as:

$$Y = \sqrt{\frac{2}{\pi e}}\, X = 0.483X \qquad \text{for large } Y$$

$$Y = \exp(\ln(8) - \gamma - \frac{2\pi}{X}) \qquad \text{for small } Y$$

[The experimental data points for data set 2.2.2 lie on a straight line between these two curves. The expression for large Y will fit the data using a different gradient: $Y = 0.045131 + 0.295X$]

7.2 Dowden

Dowden[55] produced a formula which gives a relationship between normalised power and normalised width. The asymptotic form is:

$$p = \frac{P}{k_S(T_V - T_o)\left[k_S(T_V - T_o) + k_L(T_V - T_M)\right]} = \frac{2\pi k_S(T_M - T_o)}{\left[-\gamma - \ln\left(\frac{vw}{8\kappa_s}\right)\right]\left[k_S(T_M - T_o) + k_L(T_V - T_M)\right]}$$

where:

- T_M - melting temperature (1371 °C for iron)
- T_V - vaporisation temperature (2726 °C for iron)
- T_o - ambient temperature, far from the keyhole (20 °C)
- k_S - thermal conductivity in the solid (69.4 J/m/s/°C for iron)
- k - thermal conductivity in the liquid (32.7 J/m/s/°C for iron)
- κ_S - thermal diffusivity in the solid (21.3x10^{-6}m^2/s for iron)
- - power consumed per unit depth
- v - welding speed
- w - weld width
- g - penetration depth
- γ - Euler's constant (0.5772156649)

For iron this reduces to

$$P = \frac{\eta Q}{g} = \frac{2\pi k_S (T_M - T_o)}{\left[-\gamma - \ln\left(vw/8\kappa_s\right)\right]} = \frac{5.891\times10^5}{-\gamma - \ln\left(vw/8\kappa_s\right)}$$

which gives:

$$\ln[v(mm/s)w(mm)] = \ln[8\times10^6\kappa_S] - \gamma - 589.1\frac{g(mm)}{\eta Q(W)}$$

$$\ln(vw) = 4.561 - 589.1\frac{g}{\eta Q}$$

[A plot of ln(*vw*) against $g/\eta Q$ for the data set 2.2.2 gives a straight line with a linear fit:

$$\ln(vw) = 4.2485 - 569.8\ g/\eta Q$$

The value for the width at half height was used for all data points. This equation seems to fit the data well.]

7.3 Ion[38]

The maximum welding speed *v* depends on the power *q* and the material thickness *d* according to:

$$v = \frac{kq}{d^j}$$

where *k* and *j* are constants. *k* is determined by factors that influence the process efficiency and *j* generally lies between 0.8 and 2.

7.4 Steen

Steen[56] gives a formula based on the assumption that the laser heat input forms a 2-d line source with little or no T gradient in the z-direction. For sheet welding, loss of heat by conduction is approximately a constant proportion of the input energy. So

$$\eta\ P = 0.33\, vwt\rho\, C_p \Delta T$$

where

- η = coupling coefficient, derived experimentally (Jmm^{-2})
- P = incident absorbed power (W)
- v = traverse speed (m/s)
- w = weld width (m)
- t = weld thickness (m)
- ρ = material density (kg/m^3)
- C_p = specific heat (J/kgK)
- ΔT = temperature rise to the melting point (K)

7.5 Metzbower

Metzbower[57] used dimensional analysis to produce an equation to predict penetration depth. A fit with experimental results (in all cases full-penetration welds) gave good results with the equation:

$$\ln\left(\frac{dKT_M}{P}\right) = -2.2426 - 1.2056\ln\left(\frac{vb}{\kappa}\right) \quad \text{or} \quad d = 0.10618\left(\frac{P}{KT_M}\right)\left(\frac{vb}{\kappa}\right)^{-1.2056}$$

where

- P - laser power (Watts);
- d - penetration depth (m);
- T_M - melting temperature of the alloy;
- K - thermal conductivity of the alloy at room temperature ($Wm^{-1}K^{-1}$);
- v - weldig speed (m/s);
- b - beam diameter (m);
- κ - thermal diffusivity of the alloy at room temperature (m^2/s).

References

1 Y.S. yang and S.H.Lee, 1999, Journal of Materials Processing Technology, **94**, 151-156.

2 J. Biffin, N. Blundell, T. Johnson and C. Page, 1999, Proc. 5th International Conference (1998) - *Trends in Welding Research*. Ed. J.M. Vitek, S.A. David, J.A. Johnson, H.B. Smartt, T. DebRoy. Printed 1999 by ASM International. pp 492-497.

3 F. Bachmann. Rofiin-Sinar Laser GmbH, 18.11.98.

4 J. Baron, 1994, Welding Journal, **73**, No. 7, 33-39.

5 P.W. Fuerschbach, 1996, Welding Journal, **75**, Issue 1, 24-s - 34-s.

6 L.H.J.F. Beckmann and D. Ehrlichmann, 1995, Optical and Quantum Electronics, **27**, 1407-1425.

7 J. Rapp, C. Glumann, F. Dausinger and H. Hügel, 1995, Optical and Quantum Electronics, **27**, 1203-1211.

8 N. Blundell, J. Biffin, T. Johnson and C. Page, 1999, Proc. 5th International Conference (1998) - *Trends in Welding Research*. Ed. J.M. Vitek, S.A. David, J.A. Johnson, H.B. Smartt, T. DebRoy. Printed 1999 by ASM International. pp 483-487.

9 Y. Tzeng, 2000, J. Mat. Proc. Tech., **102**, 40-47.

10 E. Schubert, M. Grupp, and G. Sepold, 1998, Laser Magazin, **2**, 14-17.

11 E. Beyer, V. Krause and P.Loosen, 1994, Journal de Physique, Vol. 4, Colloque 4, Suppl. JP 111, No. 4, C4-13.

12 E. Schubert, M. Klassen, I. Zerner and G. Sepold, 1998, Laser Magazin, **4**, 17-20.

13 A. Kar and M.D. Langlais, 1995, Optical and Quantum Electronics, **27**, 1165-80.

14 H.N. Bransch, D.C. Weckman and H.W. Kerr, 1994, Welding Journal, **73**, No. 6, 141-s - 151-s.

15 S. Chiang and C.E. Albright, 1993, Welding Journal, **72**, No. 3, 117-s - 121-s.

16 C. Limmaneevichitr and S. Kou, 2000, Welding Journal, **79**, Iss. 5, 126-s - 135-s.

17 P. Pecas, M. Henrique, R.M. Miranda and L. Quintino, 1995, Optical and Quantum Electronics, **27**, 1193-1201.

18 P.G. Klemens, 1976, J. Appl. Phys., **47**, 2165-2174.

19 S. Katayama, R. Usui, A. Matsunawa, 1999, Proc. 5th International Conference (1998) - *Trends in Welding Research*. Ed. J.M. Vitek, S.A. David, J.A. Johnson, H.B. Smartt, T. DebRoy. Printed 1999 by ASM International. pp 467-472.

20 M. Pastor, H. Zhao and T. DebRoy,1999, Proc. 5th International Conference (1998) - *Trends in Welding Research*. Ed. J.M. Vitek, S.A. David, J.A. Johnson, H.B. Smartt, T. DebRoy. Printed 1999 by ASM International. pp 455-460.

21 M. Milacic and R. Kovacevic, 1999, Proc. 5th International Conference (1998) - *Trends in Welding Research*. Ed. J.M. Vitek, S.A. David, J.A. Johnson, H.B. Smartt, T. DebRoy. Printed 1999 by ASM International. pp 449-454.

22 P.-C. Wang, 1993, Welding Journal, **72**, No. 4, 155-s - 163-s.

23 C. Prat, J.E. Montagne and M. Autric, 1994, Journal de Physique, Vol. 4, Colloque 4, Suppl. JP 111, No. 4, C4-107.

24 B.A. Mehmetli, K. Takahashi and S. Sato, 1996, Applied Optics, **35**, 3237-3242.

25 T. Dascalu, V. Lupei, N. Pavel and C. Neagu, 1994, Journal de Physique, Vol. 4, Colloque 4, Suppl. JP 111, No. 4, C4-179.

26 N.N. Rykalin, 1951, *Calculation of Heat Flow in Welding*, Translated by Zvi Paley and C.M. Adams Jr., Moscow.

27 N. Christensen, V.L. Davies and K. Gjermundsen, 1965, British Welding Journal, **12**, 54-75.

28 G. Phanikumar, R. Pardeshi, K. Chattopadhyay, P. Dutta and J. Majumder, 1999, Proc. 5th International Conference (1998) - *Trends in Welding Research*. Ed. J.M. Vitek, S.A. David, J.A. Johnson, H.B. Smartt, T. DebRoy. Printed 1999 by ASM International. pp 461-466.

29 L. Bonello, M. Cantello and G. Savant, 1995, Optical and Quantum Electronics, **27**, 1291-1301.
30 S. Tsukamoto, K. Hiraoka, Y. Asai, H. Irie and M. Oguma,1999, Proc. 5th International Conference (1998) - *Trends in Welding Research*. Ed. J.M. Vitek, S.A. David, J.A. Johnson, H.B. Smartt, T. DebRoy. Printed 1999 by ASM International. pp 431-436.
31 V.V. Semak, R.J. Steele, P.W. Fuerschbach and B.K. Damkroger, 2000, J. Phys. D, **33**, 1179-1185.
32 K.N. Lankalapalli, J.F. Tu, K.H. Leong, M. Gartner, 1999, J. Man. Sci. and Eng., **121**, 179-188.
33 H.B. Kim and C.H. Lee, 1999, Science and Technology of Welding, **4**(1), 51.
34 J.Y. Jeng, T.F. Mau and S.M. Leu, 2000, J. Mat. Proc. Tech., **99**, 207-218.
35 Y. Tzeng, 2000, J. Mat. Proc. Tech., **100**, 163-170.
36 M. Färber, 1995, Optical and Quantum Electronics, **27**, 1449-1455.
37 A. Verwaerde, R. Fabbro and G. Deshors, 1995, Journal of Applied Physics, **78**, 2981-2984.
38 J.C. Ion, 1992, *Modeling of laser material processing* in *The Industrial Laser Handbook*, 1992-93 edition, Eds. D. Belforte and M. Levitt, Springer-Verlag, New York, 39-47.
39 C. Lampa, A.F.H. Kaplan, M. Resch and C. Magnusson, 1998, Lasers in Engineering, **7**, 241-252.
40 W.M. Steen, J. Dowden, M. Davis and P. Kapadia, 1988, J. Phys. D, **21**, 1255-1260.
41 R. Akhter, M. Davis, J. Dowden, P. Kapadia, M. Ley and W.M. Steen, 1989, *J. Phys. D*, **22**, 23-28.
42 M. Resch and A.F.H. Kaplan, 1998, Lasers in Engineering, **7**, 229-240.
43 P. A. Hilton, 1995, *Optical and Quantum Electronics*, **27**, 1127-1147.
44 M.C. Tsai and S. Kou, 1988, Proc. Int. Power Beam Conf., San Diego, California, Ed. E.A. Metzbower and D. Hauser, ASM International, Materials Park, Ohio, pp131-140.
45 E.A. Metzbower, P.E. Denney, W. Pratt and H.K.D.H. Bhadeshia, 1994, Proc. Materials Processing Conference, ICALEO'94, LIA vol. 79, (Laser Institute of America: Orlando), 846-853.
46 K.N. Lankalapalli, J.F. Tu and M. Gartner, 1996, J. Phys. D, **29**, 1831-1841.
47 A. Kar and J. Mazumder, 1995, J. Appl. Phys., **78**, 6353-6360.
48 J. Dowden, M. Davis and P. Kapadia, 1985, J. Phys. D, **18**, 1987-1994.
49 J. Goldak, A. Chakravarti and M. Bibby, 1984, Met. Trans. B, **15**, 299-305.
50 J.L. Doong, C.S. Wu and J.R. Hwang, 1991, International Journal of Machine Tools and Manufacture, **31**, 607-616.
51 A. Zambon and F. Bonollo, 1994, Materials Science and Engineering A, **178**, 203-207.
52 J.C. Ion, K.E. Easterling and M.F. Ashby, 1984, Acta metall., **32**, 1949-1962.
53 B. Grabás, J. Dard-thuret and M. Laurent, 1994, Journal de Physique, Vol. 4, Colloque 4, Suppl. JP 111, No. 4, C4-139 - C4-142.
54 D.T. Swift-Hook and A.E.F. Gick, 1973, Welding Journal, **52**(11), 492-s - 499-s.
55 J. Dowden, 1985, J. Appl. Phys., **57**, 4474-4479.
56 W.M. Steen and G.J. Shannon, 1999, Proc. 5th International Conference (1998) - *Trends in Welding Research*. Ed. J.M. Vitek, S.A. David, J.A. Johnson, H.B. Smartt, T. DebRoy. Printed 1999 by ASM International. pp423-429.
57 E.A. Metzbower, 1993, Welding Journal, Iss. 8, 403-s - 407-s.